Composites Part B 178 (2019) 107478

Contents lists available at ScienceDirect

Composites Part B

journal homepage: www.elsevier.com/locate/compositesb

NaOH etching and resin pre-coating treatments for stronger adhesive bonding between CFRP and aluminium alloy

Yunsen Hu [a], Bingyan Yuan [a], Fei Cheng [a,b], Xiaozhi Hu [a,*]

[a] Department of Mechanical Engineering, University of Western Australia, Perth, WA, 6009, Australia
[b] School of Materials Science and Technology, China University of Geosciences (Beijing), Beijing, 100083, PR China

ARTICLE INFO

Keywords:
Adhesive bonding
Aluminium alloy
CFRP
Alkaline etching
Resin pre-coating

ABSTRACT

Adhesive bonding between carbon fibre reinforced plastics (CFRPs) and aluminium alloys is extensively practised to achieve optimum lightweight and reliable structures in the aerospace and automobile industries. In this research, we study pre-treatments of aluminium substrates for stronger adhesion with CFRP. An ultrasonic etching process was carried out in alkaline solutions to investigate the influence of NaOH concentration on adhesive bonding characteristics. An ultra-thin layer of acetone-diluted resin pre-coating (RPC) without hardener was then applied to the etched substrates to seal micro-cavities before adhesive bonding. The single lap shear test was used to evaluate the adhesive bond strength under different surface conditions. The topography and chemistry of treated surfaces were characterised using various surface analytical tools including optical profilometry, scanning electron microscopy and X-ray microanalysis (SEM/EDS), contact angle goniometry and X-ray photoelectron spectroscopy (XPS). Experimental results showed a maximum 91% improvement in bond strength after alkaline etching treatments, which removed the weak passive oxide layers and allowed the formation of thin hydroxide layers through aluminium-water reactions. The wettability of etched specimens was also improved, indicating by their higher surface energy values. Variations of roughness parameters and tomography under different NaOH concentrations also affected the bond strength. The RPC treatments further increased the bond strength of NaOH etched specimens by 8.4–11.6%. The surface treatments reported in this work are very simple and cost-effective for producing durable adhesive joints in industrial applications.

1. Introduction

Structural adhesive joints between carbon fibre reinforced plastics (CFRPs) and aluminium are extensively used in engineering structures from the aerospace industry, e.g. hull segments, to the automobile industry, e.g. CFRP roof frames [1–5]. They have many advantages compared with conventional mechanical fastening methods such as using bolts and nuts, screws and ri which may induce thermal and mechanical damages to the composites during the drilling process [6–8]. Additionally, CFRP and aluminium can form a strong galvanic couple, resulting in electrochemical corrosion of aluminium if mechanical fasteners are used [9–11].

Adhesive bonding has the ability to join dissimilar materials with varying thicknesses and large area without causing significant stress concentrations [12]. The potential corrosion issue between CFRP and metal substrates can be prevented by introducing a thin non-conductive fibre layer such as Aramid or using a thick adhesive layer to avoid direct contact between substrates [13,14]. The strength of adhesive-joined CFRP and aluminium strongly depends on the metal/polymer interface due to relatively weak intermolecular forces between the resin and passive oxide layer [15]. In order to enhance the bonding performance, surface pre-treatments of aluminium are essential and can be accomplished by either physical (sanding, grinding, abrasive blasting etc.) or chemical methods (anodization etc.) [13,16–20].

Alkaline etching is a common treatment processes for removing the mechanically weak surface oxide layers of aluminium alloys. It also results in a scalloped surface morphology [21], which can potentially improve the mechanical adhesion. However, there have been comparatively few studies examining the effects that alkaline etching can have on adhesive bonding. Saleema et al. treated AA 6061 substrates with the 0.1 M NaOH solution in an ultrasonic bath for varying times of immersion. They concluded that the adhesive bond strength could be improved by approximately 60% due to the rough microscale surface texture [22]. Zain et al. modified the polished AA 2024-T3 surfaces with 5% (1.2 M)

* Corresponding author.
E-mail address: xiao.zhi.hu@uwa.edu.au (X. Hu).

https://doi.org/10.1016/j.compositesb.2019.107478
Received 26 May 2019; Received in revised form 21 September 2019; Accepted 22 September 2019
Available online 23 September 2019
1359-8368/

NaOH solution for 5 min and applied different polyurethane (PU) adhesives to the adherends. They found that the lap shear strength of treated specimens increased roughly 55% more than the untreated aluminium, and this improvement was solely correlated to the wettability of aluminium surfaces [23]. Both studies showed increased adhesive bond strength after NaOH etching, but the mechanisms they deduced were different. This was likely caused by the different processes and substrates they used.

According to the mechanical interlocking theory, adhesion occurs by the penetration of adhesives into cavities, pores, and other irregularities of the substrate surface [24]. Therefore, the extent of penetration plays a crucial role in affecting the adhesive bonding of treated aluminium. The penetration of adhesive depends on many factors such as cavity dimensions, surface roughness, surface energy and viscosity of the adhesive [24,25]. In order to increase the penetration depth, a unique technique using acetone as a solvent to dilute the high-viscosity epoxy adhesive (without hardener), namely, resin pre-coating (RPC) was developed. Acetone is a common solvent with a low viscosity at room temperature, which increases the tendency for penetration of micro-cavities. Previous studies have demonstrated that the RPC technique can be used for improving adhesive bonding of grit-blasted steel [18,20], engineered bamboo [26] and granite [27]. Alkaline etched aluminium surfaces have fewer and smaller cavities than those substrates. The effectiveness of RPC treatments on these kinds of surfaces have not been tested.

To the best of the authors' knowledge, no research has been done to determine the influence of NaOH concentration on bonding performance of etched aluminium alloys. In this study, AA6060 T5 substrates were etched in 0.1/0.5/1.0 M NaOH solutions and adhesively bonded to carbon fibre composites. Single lap shear tests were performed to measure the bond strength. Several characterisation techniques were used to observe changes in properties including surface morphology, roughness, wettability and chemical composition of aluminium substrates before and after the etching process. The RPC technique was also applied to the NaOH-treated specimens to evaluate its effectiveness on alkaline etched micro-rough surfaces.

2. Material and methods

2.1. Materials and sample preparation

Commercial available 3 mm thick 6060 T5 aluminium flat bars (Midalia Steel Pty Ltd., Australia) and 2 mm thick cross-ply $[0/90]_{6s}$ CFRP plates with 3K twill weave outer layers made of T300 fibres (Carbonwiz Technology Co., Ltd., China) were cut into pieces with a dimension of 101.6*25.4 mm. They were ultrasonically cleaned in acetone (AR, Chem-Supply Pty Ltd., Australia) for 45 min to remove contaminants including dirt, dust and oil. The degreased aluminium substrates were ultrasonically etched in 0.1/0.5/1.0 M NaOH solutions (made from NaOH Pellets, AR, supplied by Chem-Supply Pty Ltd., Australia) at 55 °C for 10 min and then immersed in deionised water at ambient temperature for 10 min to stop the reaction. Some dark-brown powders may be attached to the substrates, particularly when using concentrated NaOH solutions as etching agents. These powders were brushed out carefully to ensure surface cleanliness before adhesive bonding. After etching, aluminium substrates were further cleaned ultrasonically in acetone for 10 min, which helps remove remaining powders on the surfaces and speed up the drying process as acetone evaporates much faster than water.

Selleys Araldite Super Strength bi-component epoxy adhesive (mainly bisphenol A epichlorohydrin epoxy resin and triethylenetetramine hardener, supplied by DuluxGroup Pty Ltd., Australia) was selected for the adhesion and RPC processes. The RPC technique involves immersing etched aluminium substrates in a solution consisting of acetone (90 vol%) and epoxy resin (10 vol%, without hardener) for 10 s to form coatings on the micro-rough surfaces. The diluted epoxy resin can easily reach the bottoms of pits and gullies where typically high-viscosity adhesives cannot flow into, as sketched in Fig. 1. Excess liquid was spun out to minimise the amount of resin-acetone solution left on the surface. Resin and hardener mixture was then applied to join aluminium and CFRP substrates after evaporation of the acetone. The influence of RPC on the mixing ratio of resin and hardener is negligible since only an extremely small amount of resin was left on the substrate (approximately 1 mg over an area of 6.25 cm^2). Resin pre-coatings cured simultaneously with the epoxy adhesive through diffusion and acted as interlocks to prevent de-bonding at the aluminium/adhesive interface. It took 72 h for the epoxy adhesive to reach the maximum bond strength at 60 °C before mechanical testing.

2.2. Experimental methods

The contact angles (CAs) between aluminium surfaces and liquids were measured by a DMo-501 droplet contact angle meter (KYOWA Interface Science Co., Ltd., Japan) using a sessile drop technique. The droplet size was 2 μL. Three measurements were made for each surface condition. The surface free energies (SFEs) of aluminium samples were calculated using the Owens-Wendt-Rabel-Kaelble (OWRK) method (1), which divides the SFE of a solid into dispersive and polar components. Water and 1-bromonaphthalene were chosen as the test liquids. The SFE values and parameters are shown in Table 1.

$$\gamma_S = \gamma_S^D + \gamma_S^P \tag{1}$$

where γ_S is the SFE of solid; γ_S^D is the dispersion component of solid SFE; γ_S^P is the polar component of solid SFE. Values of γ_S^D and γ_S^P are calculated from equations (2) and (3).

$$\gamma_{LW}(1 + cos\theta_W) = 2\left(\gamma_S^D \gamma_{LW}^D\right)^{\frac{1}{2}} + 2\left(\gamma_S^P \gamma_{LW}^P\right)^{\frac{1}{2}} \tag{2}$$

$$\gamma_{LB}(1 + cos\theta_B) = 2\left(\gamma_S^D \gamma_{LB}^D\right)^{\frac{1}{2}} + 2\left(\gamma_S^P \gamma_{LB}^P\right)^{\frac{1}{2}} \tag{3}$$

where γ_{LW} is the SFE of water; θ_W is the measured CA of water; γ_{LW}^D is the dispersion component of water SFE; γ_{LW}^P is the polar component of water SFE; γ_{LB} is the SFE of 1-bromonaphthalene; θ_B is the measured CA of 1-bromonaphthalene; γ_{LB}^D is the dispersion component of 1-bromonaphthalene SFE; γ_{LB}^P is the polar component of 1-bromonaphthalene SFE.

The morphologies of the aluminium surfaces before and after the etching process were revealed by a scanning electron microscope (FEI Verios XHR SEM, Thermo Fisher Scientific Inc., USA) with an Everhart-Thornley detector (ETD) at 10 kV/0.4 nA. The compositions of some intermetallic particles observed in SEM images were analysed using an 80 mm^2 X-Max SDD EDX detector and Aztec (version 3.0) software (Oxford Instruments Plc, UK).

X-ray Photoelectron Spectroscopy (XPS) spectra were obtained using the ESCALAB 250Xi (Thermo Fisher Scientific Inc., USA) with an Al Kα (hv = 1846.6 eV) monochromatic radiation source at a normal take-off angle. High-resolution spectra of Al 2p and C 1s peaks were recorded with a spot size of 400 μm using 50 eV pass energy and 0.1 eV step size. Before curve fitting, the binding-energy scale was calibrated relative to adventitious hydrocarbons with a binding energy of 284.8 eV. High-resolution scans of Al 2p were analysed using XPSPEAK (version 4.1) software. The peaks were fitted after Shirley-type background subtraction, using a mixed Gaussian (70%)–Lorentzian (30%) line shape.

3D surface roughness was measured by an Altisurf 520 profilometer (Altimet SAS, France) using a CCS Prima confocal displacement sensor (CL3, Schmitt Industries, Inc., Portland). The spot size, normal and lateral resolution of the sensor are 4 μm, 25 nm and 2 μm, respectively. Measurements were made for 201 points in the x-direction and 201 points in the y-direction on an area of 2*2 mm^2. The data were subsequently analysed using TalyMap Gold (version 4.1.24974, Labindia Instruments Pvt. Ltd., India) to obtain the area roughness parameters.

Single lap shear tests were carried out to measure the strength of

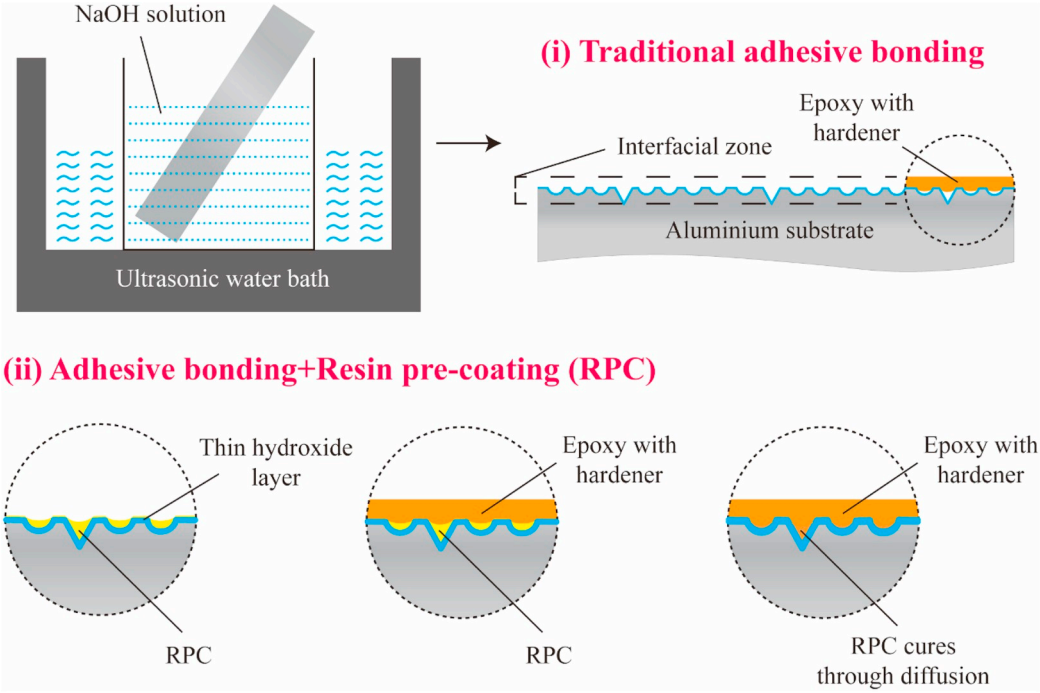

Fig. 1. The interfacial reinforcing mechanism of NaOH etching and RPC treatments.

Table 1
Surface tension components of the test liquids (mJ/m^2) [28].

Liquid	γ_L	γ_L^D	γ_L^P
Water	72.8	21.8	51
1-bromonaphthalene	44.4	44.4	0

adhesively bonded joints between CFRP and aluminium using the Instron 5982 universal testing machine (Instron Corp., USA) and a 100 kN standard tensile fixture. Specimen dimensions, bond line thickness and area specified in ASTM D5868 are illustrated in Fig. 2. During testing, specimens were loaded in tension at a constant rate of 1 mm/min. The load and crosshead displacement were automatically recorded every 0.1 s. At least six specimens were tested for each type of surface treatments. The bond strength was calculated by dividing the breaking load by the area of adhesive.

2.3. Finite element analysis (FEA) of adhesive stresses

A 3D geometrically-nonlinear FEA was implemented with the commercial software Abaqus 2019 (Dassault Systèmes, France) to investigate the stress distributions of the adhesive layer at different loads. The geometry of the finite element model was same as those of the single lap specimens used in mechanical testing. The 45° triangular spew fillets at the free edges of the specimens were also taken into account, which decreased the maximum stresses in the joint [29,30]. Material properties of the aluminium adherend and the epoxy adhesive were defined by isotropic elastic-plastic models, and the CFRP was treated as a linear-elastic orthotropic material. The stress–strain curves of aluminium and adhesive (Fig. 3) were obtained using dogbone shaped specimens according to ASTM E8 and D638, respectively. The in-plane tensile properties of CFRP were measured experimentally according to ASTM D3039, and the remaining properties were estimated based on literature [31]. The material properties employed for the simulation are summarised in Table 2. The end of the aluminium adherend was completely constrained while the end of CFRP was allowed to extend in the longitudinal direction under different loads. Tie constraints were applied to the interfaces between the adhesive and adherends. The adhesive and adherends were meshed using eight-node 3D linear brick (C3D8) elements. To improve the accuracy of the analysis, finer mesh was used near the ends of overlaps where high stress gradients are present. Fig. 4 shows the mesh of the joint region.

3. Results and discussion

3.1. Scanning electron microscopy and energy-dispersive X-ray spectroscopy

The SEM images of aluminium surfaces before and after alkaline etching are presented in Fig. 5. The as-received aluminium surface (Fig. 5 a) had a parallel valley structure arising in the extrusion process.

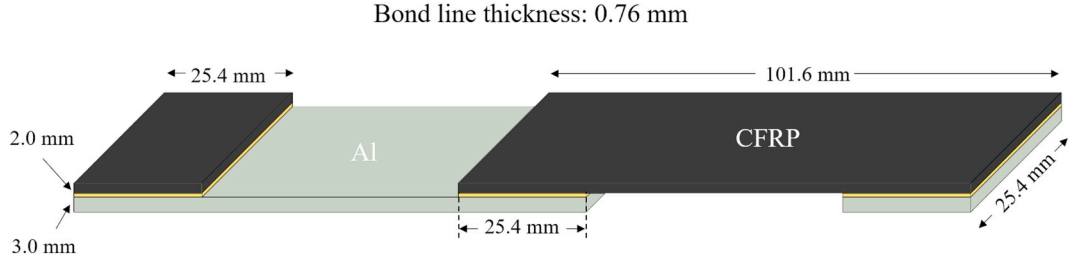

Fig. 2. Sketch of single lap shear specimens according to ASTM D5868.

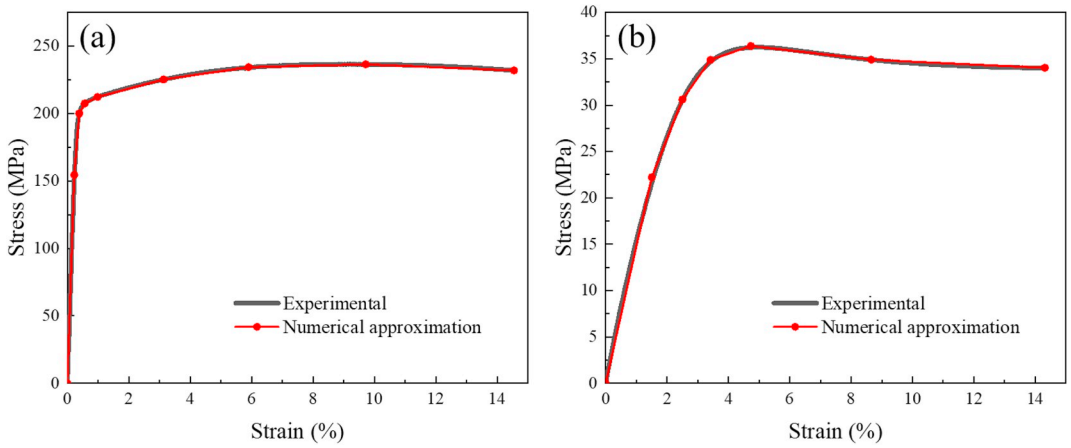

Fig. 3. Experimental and numerical stress-strain curves of (a) aluminium and (b) adhesive.

Table 2
Material properties used in simulation.

Material	E_x (GPa)	E_y (GPa)	E_z (GPa)	ν_{xy}	ν_{xz}	ν_{yz}	G_{xy} (GPa)	G_{xz} (GPa)	G_{yz} (GPa)
CFRP	73.5	73.5	12.0	0.10	0.10	0.10	4.5	4.0	4.0
Al	68.0	-	-	0.33	-	-	-	-	-
Adhesive	1.5	-	-	0.33	-	-	-	-	-

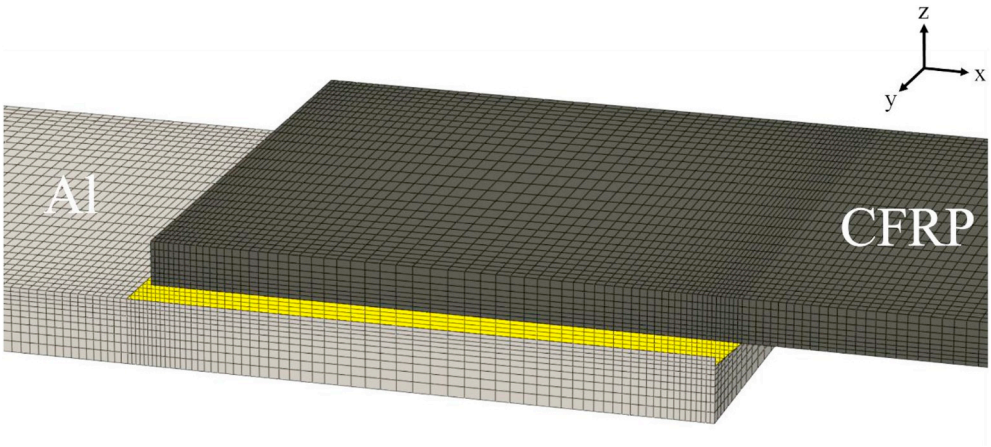

Fig. 4. Finite element mesh of the joint region.

Some horizontal scratches and friction marks generated during handling, storage, and transportation were also observed. The surface etched in 0.1 M NaOH solution (Fig. 5 b) exhibited a pitted topography, which is the typical feature of an aluminium alloy etched in alkaline solutions. The corrosion rate along the grain boundaries was higher than others, resulting in the formation of mud-crack patterns. Increasing the concentration of NaOH to 0.5 M accelerated the reaction rate and caused a more scalloped topography (Fig. 5 c).

Several intermetallic particles were exposed on the surfaces after the selective dissolution of sub-surface layers in 0.1 and 0.5 M NaOH solutions. The compositions of these particles were examined by EDX and summarised in Table 3. Since the size of the interaction volume might be greater than that of intermetallic particles, surface metal hydroxides and bulk aluminium could affect the elemental compositions determined by EDX. These iron-containing intermetallics acted as cathodic sites and promoted the anodic dissolution of aluminium [32].

A large number of submicro-cracks and micro-cracks were randomly distributed on the surface etched in 1.0 M NaOH solution (Fig. 5 d). These cracks likely resulted from stress corrosion cracking (SCC) and hydrogen embrittlement (HE) caused by alkaline exposure with high pH values. The near-surface tensile stress was produced by lattice contraction during dissolution. According to Çapraz et al., this tensile stress increases with increasing concentrations of NaOH [33]. Most of the intermetallic particles were present both below and slightly above the surface, indicating that the dissolution of iron-containing intermetallic compounds occurred in 1.0 M NaOH solution. It also caused the formation of dark-brown iron-rich powders attached to the substrate after the etching process, which may reduce the dissolution rate of the underlying aluminum substrates. Moreover, the dissolution of exposed iron-containing intermetallics led to a significant decrease in the micro-galvanic reaction rate. As a result, the pitting of the surface was inconspicuous compared with the pitting corrosion in low-concentration NaOH solutions.

3.2. *X-ray photoelectron spectroscopy*

The XPS survey spectra of as-received and etched aluminium substrates shown in Fig. 6 indicates the presence of Al, O, Mg, Si and Cu.

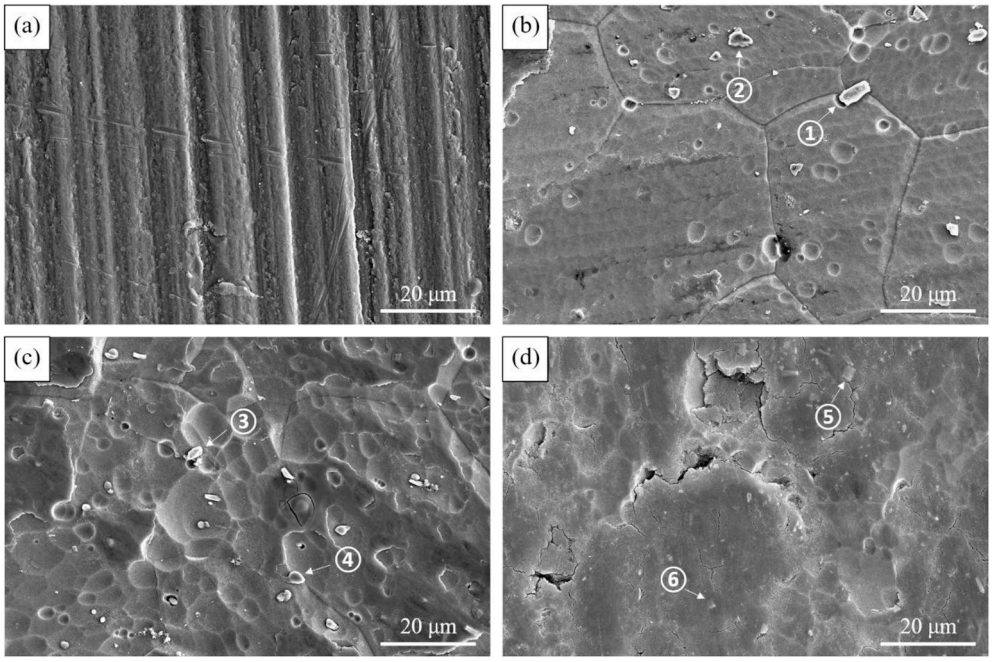

Fig. 5. SEM images of (a) as-received and (b) 0.1 M, (c) 0.5 M, (d) 1.0 M NaOH etched 6060 T5 aluminium alloy surfaces.

Table 3
EDX elemental analysis of intermetallic particles.

Spectra	Al	Fe	O	Si	Cu	Mg	S	Cl	Na	Ca
1	41.3%	36.1%	15.6%	6.5%	-	-	0.2%	0.3%	-	-
2	32.6%	24.5%	25.5%	5.7%	-	5.3%	1.2%	1.0%	2.6%	0.9%
3	29.6%	39.3%	20.1%	5.1%	4.4%	-	0.7%	0.4%	-	0.4%
4	45.0%	32.0%	12.2%	10.3%	-	-	-	0.3%	-	0.2%
5	26.8%	42.5%	32.5%	3.5%	-	-	0.3%	0.4%	-	-
6	29.2%	29.5%	26.1%	3.0%	2.2%	5.9%	0.7%	0.6%	1.7%	0.3%

These elements are the basic components of 6060 aluminium alloy. The C 1s peak was assigned to some adventitious hydrocarbon contamination of the surface.

In order to investigate the changes in native oxide layer following treatments with NaOH, the high-resolution Al 2p core-level spectra of each set of samples were analysed. The Al 2p spectrum of the as-received surface (Fig. 7 a) was composed of three distinct peaks corresponding to metallic aluminium Al_{met} (72.8 eV) [34], aluminium oxide Al_{ox} (74.8 eV) [35], aluminium hydroxide and oxy-hydroxide Al_{oh} (74.4 eV) [36]. The formation of aluminium hydroxide (oxy-hydroxide) was caused by water vapour in the atmosphere. These particles were poorly bound and considered to impair the adhesion. The thickness of this passive layer was less than the sampling depth for XPS (few nanometres) since the signal from aluminium matrix can still be detected.

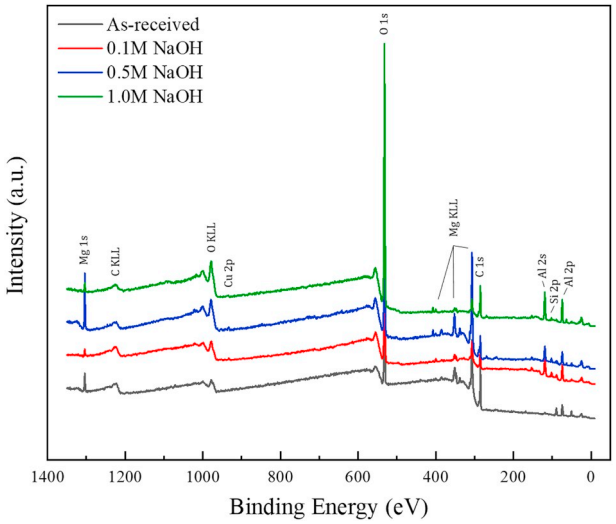

Fig. 6. Survey spectra of the 6060 T5 aluminium alloy surfaces.

For the etched samples shown in Fig. 7 b-d, there was no aluminium oxide left on the surfaces layer as they had reacted with NaOH solutions. Also, the binding energies of metallic aluminium were observed to shift from 72.9 eV to 72.0 eV, indicating that the peak was related to the intermetallics present on the surface rather than aluminium matrix. The metallic aluminium peaks became negligible in the spectrum of 0.5 M NaOH etched surface (Fig. 7 c) and disappeared in the spectrum of 1.0 M NaOH etched surface (Fig. 7 d).

Based on the percentage shares of Al_{met}, Al_{ox} and Al_{th} atoms forming the surface layers presented in Table 4, it can be found that the metallic aluminium content within the depth of analysis decreased as the NaOH concentration was increased. It was likely caused by the reaction between intermetallics and concentrated NaOH solutions, which was also observed from SEM images. The NaOH etched surfaces were predominantly composed of aluminium hydroxide within the depth of analysis. The nano-scale hydroxide layer was most likely the product of aluminium-water reaction during the deionised water cleaning process following complete removal of the passive oxide layer in NaOH solutions [37,38].

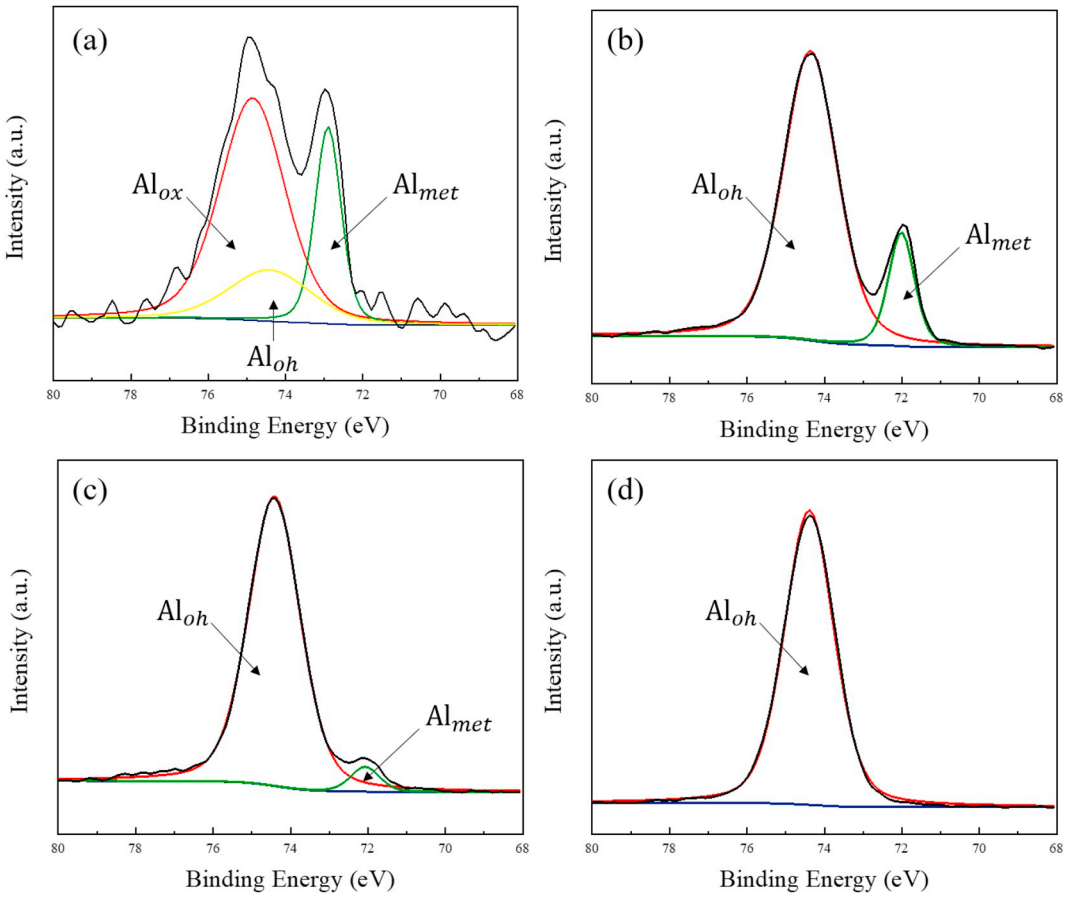

Fig. 7. High resolution Al 2p core-level spectra for the 6060 T5 aluminium alloy surfaces (a) as-received and etched in (b) 0.1 M, (c) 0.5 M, (d) 1.0 M NaOH solutions.

Table 4
Surface elemental composition of the thin surface layer from XPS data.

Treatments	Al_{met}	Al_{ox}	Al_{oh}
As-received	21.5%	61.0%	17.5%
0.1 M NaOH	15.9%	-	84.1%
0.5 M NaOH	4.6%	-	95.4%
1.0 M NaOH	-	-	100.0%

3.3. Surface roughness

Surface height parameters in accordance with ISO 25178 are given in Table 5, where Sa is the surface arithmetical mean roughness, Sq is the surface root mean square roughness, Sp is the maximum peak height, Sv is the maximum pit height, Sz is the maximum height, Ssk is the skewness and Sku is the kurtosis. Fig. 8 presents the 3D images of surface height values obtained with a confocal surface topometry system.

The as-received surface (Fig. 8 a) showed a parallel valley structure arising from the aluminium extrusion process, which had a limited contribution to the adhesive strength of a single lap joint as these ridges were oriented along the direction of motion. After etching with 0.1 M NaOH solution (Fig. 8 b), the extrusion marks became less visible and the surface roughness values Sa and Sq also decreased slightly. Treatments with 0.5/1.0 M NaOH solutions (Fig. 8 c/d) resulted in further removal of extrusion marks and creation of randomly micro-rough surfaces. The maximum surface roughness values were obtained when etched in 0.5 M NaOH solution due to the highest pitting corrosion rate illustrated by SEM images (Fig. 5). The exposed iron-containing intermetallics were dissolved in 1.0 M NaOH solution, resulting in less severe micro-galvanic reaction and the formation of iron-rich powders attached to the substrate. Therefore, the pitting corrosion rate of the underlying aluminium substrates was decreased, which resulted in a lower roughness values compared to that of the 0.5 M NaOH etched surface.

Table 5
Surface height parameters of the 6060 T5 aluminium alloy surfaces.

Sample	Sa (μm)	Sq (μm)	Sp (μm)	Sv (μm)	Sz (μm)	Ssk	Sku
As-received	2.01	2.60	59.70	20.10	79.80	1.30	29.40
0.1 M NaOH	1.99	2.47	9.97	9.74	19.70	0.08	2.87
0.5 M NaOH	2.71	3.42	16.70	35.70	52.40	0.10	3.64
1.0 M NaOH	2.27	2.88	19.70	27.30	46.90	0.03	4.83

Variances in Sp, Sv and Sq were caused by manufacturing defects. The high Ssk and Sku values of as-received substrate indicated that the height distribution was highly skewed in the positive direction and heavy-tailed. The height distributions of etched substrates were approximately symmetric as their skewness values were closed to 0.

3.4. Contact angle test

The average CAs of samples with different surface treatments are presented in Fig. 9. The measurements showed that the CAs of water and 1-bromonaphthalene decreased to 71.7° and 41.8° on the 0.1 M NaOH etched surfaces, as compared to 93.6° and 51.9° on the as-received surfaces, respectively. After being treated with 0.5 M NaOH solutions, the water and 1-bromonaphthalene CAs on aluminium surfaces further decreased to 62.7° and 33.6°, respectively. Both CAs reached the

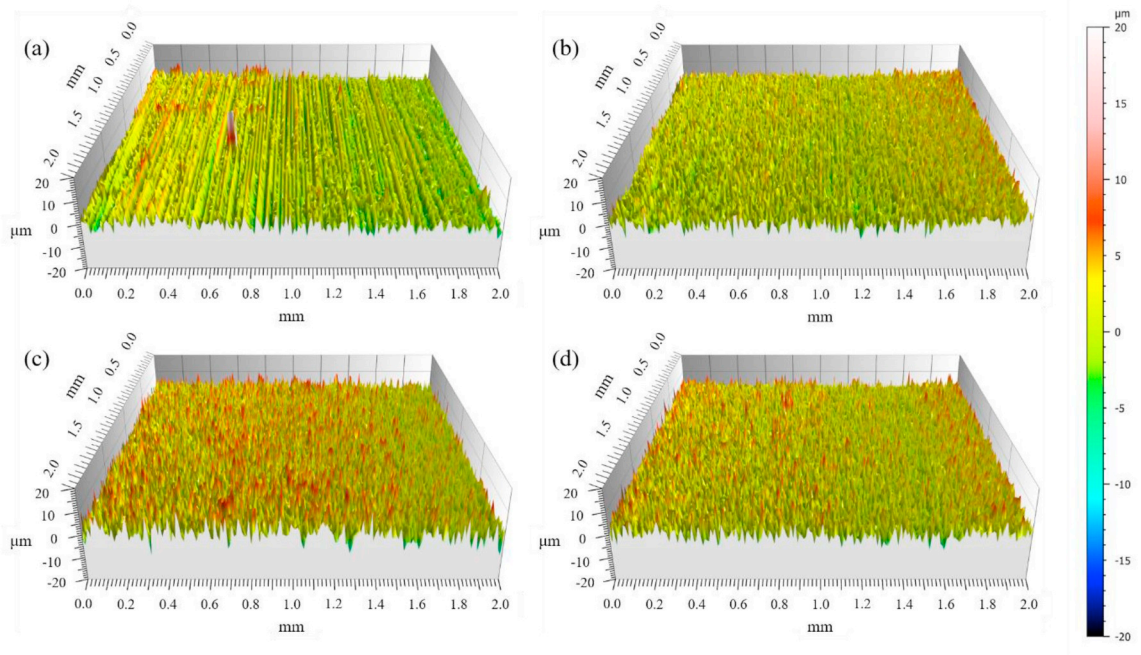

Fig. 8. 3D presentation of surface height profiles of the 6060 T5 aluminium alloy surfaces (a) as-received and etched in (b) 0.1 M, (c) 0.5 M, (d) 1.0 M NaOH solutions.

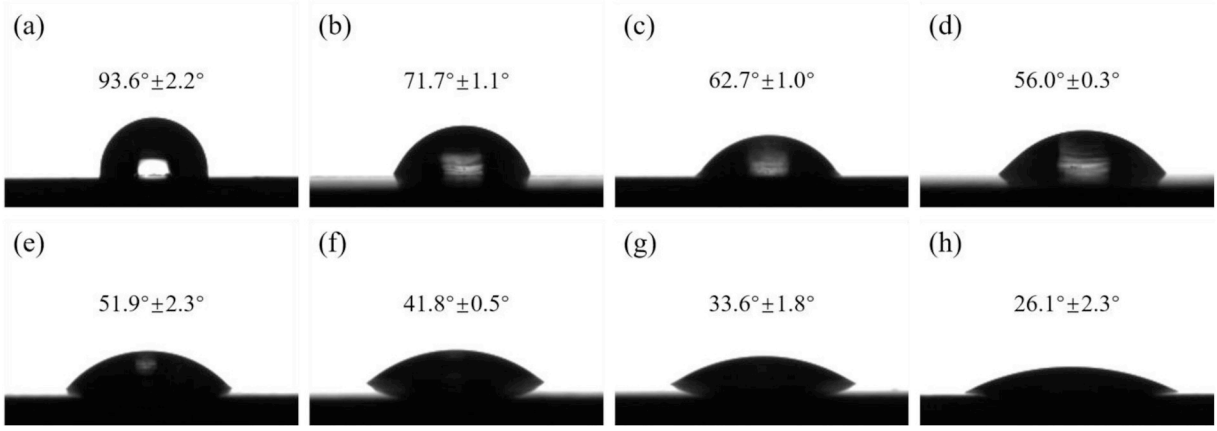

Fig. 9. Contact angles of (a–d) water, (e–h) 1-bromonaphthalene on (a, e) as-received and (b, f) 0.1 M, (c, g) 0.5 M, (d, h) 1.0 M NaOH etched 6060 T5 aluminium alloy surfaces.

minimum values on the surfaces treated with 1.0 M NaOH solutions.

The surface free energies (SFEs) were calculated from these CAs using the Owens-Wendt-Rabel-Kaelble method, and the results are given in Table 6. The analysis of the SFE results showed that the lowest SFE value was obtained for the as-received surfaces, and the highest SFE value was found for the 1.0 M NaOH etched surfaces. The higher concentration of NaOH solutions used in the etching process increased the SFEs of aluminium substrates and therefore, achieved better wettability. The improvements of SFE were mainly due to the formation of thin hydroxide layer and the removal of contaminants during etching and cleaning processes. Surface roughness at micro and nano-scales also have influence on CAs, resulting in variations in the SFEs of etched substrates [39]. Regarding the individual components of the overall SFEs, the dispersion components were greater than polar components for all substrates. In the case of the lowest SFE value for the as-received surfaces, the polar component comprised only 5.1% of the SFE. However, this proportion amounted to 19.9–26.6% for the NaOH etched surfaces.

Table 6
SFEs (mJ/m^2) obtained using OWRK method.

Treatments	γ_S^D	γ_S^P	γ_S
As-received	29.0	1.6	30.6
0.1 M NaOH	33.8	8.4	42.2
0.5 M NaOH	37.3	11.8	49.1
1.0 M NaOH	40.0	14.5	54.5

3.5. Single lap shear test

Results obtained from single lap shear tests are presented in Fig. 10. The bond strength between CFRP and aluminium was significantly improved after alkaline etching treatments. In particular, specimens treated with 0.1 M NaOH exhibited the maximum bond strength of 18.43 MPa, which was 91% higher than the strength of as-received specimens. These improvements can be partially explained by the

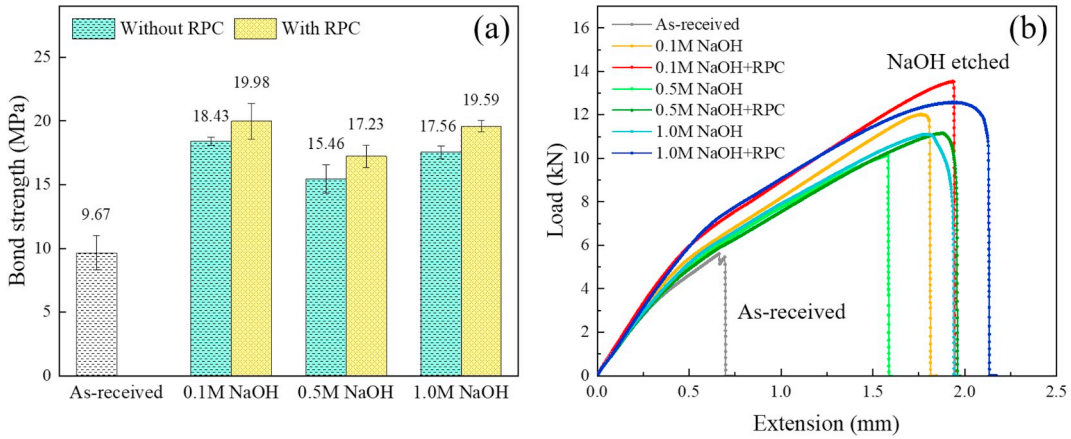

Fig. 10. Single lap shear test results: (a) average bond strength and (b) representative load-extension curves.

replacement of the mechanically weak native oxide layers. The formation of thin aluminium hydroxide layers increased the SFEs, which assured greater surface contact and helped achieve stronger interfacial bonding.

Surface roughness was also found to have a significant influence on the adhesion strength. The relationship between the surface roughness and adhesive bond strength is not simple. The increase in surface roughness enlarges the effective bonding area. However, excessive numbers of irregularities tend to trap air bubbles and cause insufficient wetting of the surface [40,41]. The optimal surface roughness for adhesion depends on many factors, including the chemical properties of the adherend and adhesive materials and the bondline thickness [42–44]. Budhe et al. investigated the influence of surface roughness on the adhesive bond strength using AA6061 and Araldite 2015 adhesive. They reported that the optimal Ra value was found in the range of 1.75–2.5 μm [42]. Ghumatkar et al. conducted follow-up experiments using AA6063 instead of AA6061. They found that the optimal Ra value for maximum bond strength was 2.05 μm [43], which is close to the roughness value of 0.1 M NaOH etched substrate. Although the substrates etched in 0.5 M NaOH solution had the second highest SFE, their roughness values were too high to allow proper wetting of the surface, resulting in lower bond strength. The protruding intermetallics and shallow cracks on 0.1 M NaOH etched surfaces can contribute to better mechanical interlocking between adhesives and adherends. Its moderate roughness parameters also prevent insufficient wetting and therefore, assured the highest bond strength. The substantial number of micro and submicro-cracks in 1.0 M NaOH etched substrates were difficult to wet. Moreover, the adhesive interlocking to these narrow cracks may not be as effective as that to the pits and wide cracks present on the 0.1 M NaOH etched surfaces. But the SFE values of 1.0 M NaOH etched substrates still allowed for a bond strength comparable to that of the 0.1 M NaOH etched substrates.

Specimens treated with RPC technique showed further improvements in bond strength. RPC increased the bond strength of NaOH etched specimens by 8.4–11.6%, which were lower than the values found in previous studies. Wang et al. reported an improvement of 25% on grit-blasted steel surface [18]. Liu et al. reported an improvement of 130% on engineered bamboo surfaces [26]. The discrepancy is mainly caused by the different amounts of micro-cavities and irregularities present on the surfaces. The surface of NaOH etched aluminium is smoother than that of the grit-blasted steel and engineered bamboo, leading to an acceptable wettability without the help of RPCs. However, the process is still useful due to its simplicity and excellent cost-effectiveness.

The lap shear values obtained on the surface treated with NaOH and RPC is comparable to those obtained by some common surface treatment methods, such as sand-blasting. Arenas et al. reported a maximum joint strength of 18.81 MPa between sand-blasted AA6160 and carbon fibre composite using Loctite 9466 epoxy adhesive [17]. In comparison with sand-blasting, NaOH etching and RPC treatments do not damage the substrates and are applicable to thin aluminium parts in composite structures, such as aluminium honeycombs for automotive and aerospace applications [45–47]. The lap shear test results were obtained at room temperature. Changes in temperature may cause a decrease in bond strength due to the difference in thermal expansion between adhesives and adherends, and variation in adhesive mechanical properties at different temperatures [48]. Selecting and testing the appropriate adhesive is required for specific applications.

The typical failure modes of single lap shear specimens are presented in Fig. 11. The as-received specimen showed predominant adhesive failure at the metal-adhesive interface caused by the mechanically weak natural oxide layer and improper wetting of the surface. However, adhesive failures also occurred at the interfaces between adhesive and CFRPs in specimens treated with NaOH solutions. It indicated that the interfacial bonding strength between adhesive and aluminium was significantly improved after etching procedures. The RPC technique can further enhance the interfacial bonding performance between adhesive and aluminium, which was evident from the larger de-bonded areas and cohesive damage observed on the composite sides of specimens shown in Fig. 11 c, e, and g. Surface treatments of the composite substrate may help achieve higher bond strength by reducing adhesive failures.

The SEM images of ruptured surfaces between the epoxy adhesive and aluminium alloys are shown in Fig. 12. The surface treated in 0.1 M NaOH solution without using RPC technique (Fig. 12 a,c) exhibited a complete adhesive failure. No epoxy residue remained in the cracks or pits, which suggested that the high-viscosity adhesives used in this research were not able to make intimate contact with these micro-rough surfaces. By contrast, the specimen treated with RPC technique showed plenty of epoxy residue adhered to the surface (Fig. 12 b). Some of the pits and cracks along grain boundaries were filled with epoxy resin (Fig. 12 d), which proved that the acetone diluted adhesives could easily reach greater penetration depth in micro-cavities and act as interlocks. The RPC technique also helped change the failure mode from complete adhesive failure to partial cohesive failure at the micron scale, therefore, achieving higher bond strength.

3.6. Finite element analysis of stress distributions

Geometrically-nonlinear FEA was implemented to study the adhesive stresses along a straight line passing through the middle of the adhesive layer under different loads before damage initiation, and the results are shown in Fig. 13. These loads were chosen based on the experimental observations that the specimens without surface treatments failed at loads around 6 kN, and the treated specimens can withstand loads up to

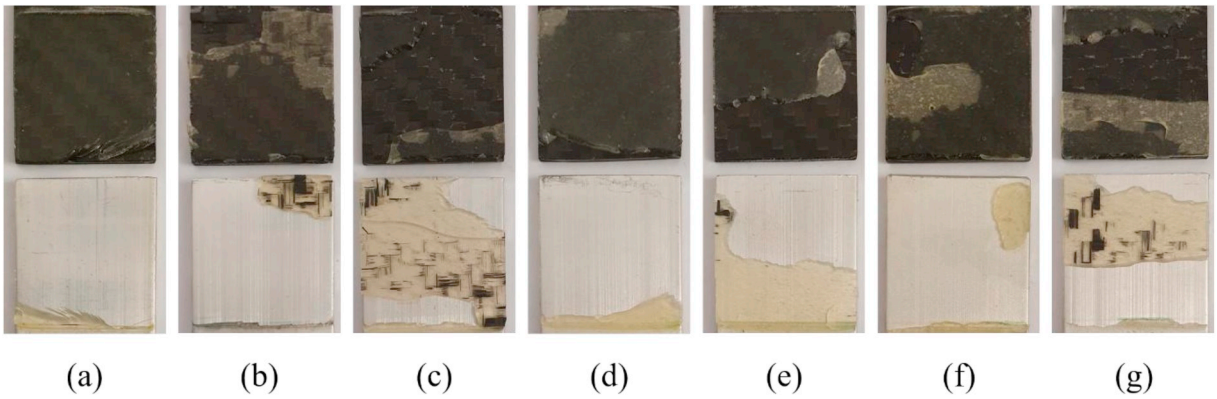

Fig. 11. Images of ruptured surfaces (c,e,g) with RPC, (a,b,d,f) without RPC, (a) as-received, etched in (b,c) 0.1 M, (d,e) 0.5 M, (f,g) 1.0 M NaOH solutions.

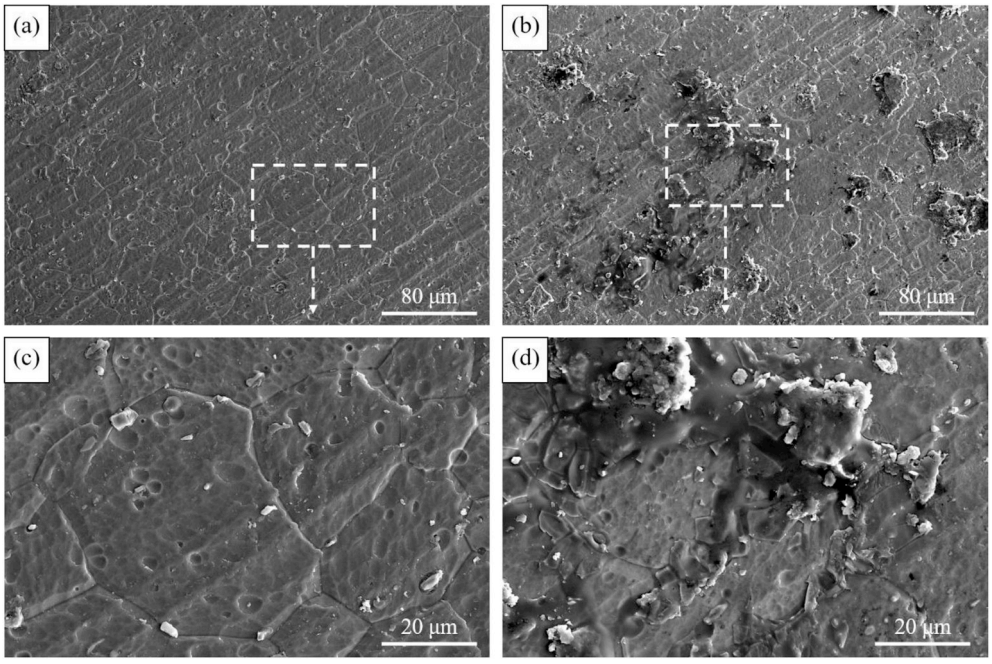

Fig. 12. SEM images of ruptured surfaces (a,c) without RPC, (b,d) with RPC. Clearly, RPC enhanced bonding strength by promoting cohesive failure.

13 kN.

Owing to load eccentricity, single lap joint adherends bent during the loading, introducing large peel stresses at the ends of the overlap and compressive stresses in-between. The peel and shear stresses on the right-hand (composite) side of the adhesive were higher due to unbalanced adherends. The maximum peel stresses were found near the ends

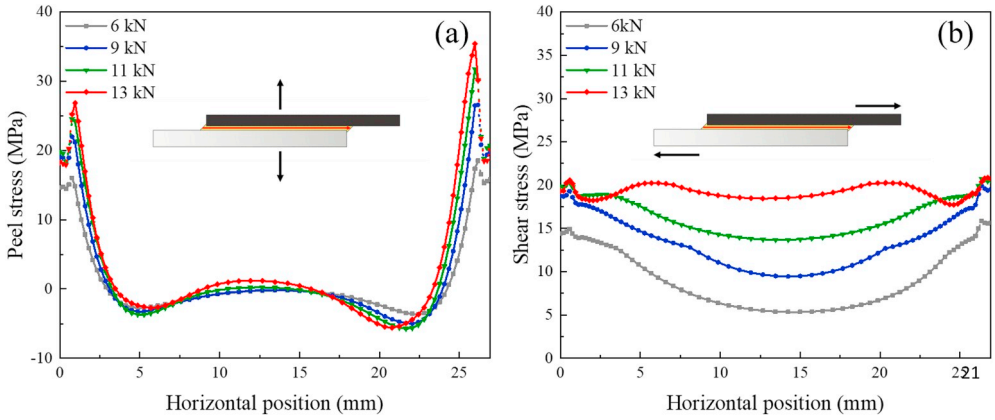

Fig. 13. Distributions of (a) peel and (b) shear stresses along the middle line of the adhesive, dotted lines at both ends of the curves indicate the stresses in the spew fillets.

of the overlap region rather than the spew fillets, which satisfied the traction free boundary condition. The maximum shear stresses occurred in the fillets. These fillet effectively reduced the stress concentration at the free edges of the joint and allowed a smooth transition to inner regions of the overlap [49]. The peel stresses were typically much higher in magnitude than the shear stresses close to the free edges and kept increasing with increase in applied load until it reached the ultimate strength of the adhesive.

Specimens failed at lower loads (6–9 kN) did not appear to experience significant plastic deformation since the analytical stresses were lower than the yield strength. The initiation of damage was more likely to occur at the interfaces between aluminium and adhesive. Local plastic deformation was observed at the free edges of adhesive layers in the specimens subjected to higher load levels (11–13 kN), which also caused the redistribution of shear stresses. The shear stresses in the inner region of the overlap were significantly increased while those at the free edges remained almost unchanged. The failure could initiated by the interfacial bond failure between the adhesive and the adherends or by the adhesive fracture in a relatively ductile manner near the spew fillets.

According to the simulated results, the peak peel stresses around the local stress concentrations were nearly one time higher than the average bond strengths calculated by dividing the maximum load by the bond area due to the large bending deformation of adherends. Specimens were more likely to fail due to large peel stresses near the free ends. Therefore, the single lap shear test results were only used for comparative purposes. It did not give a true measure of the shear strength.

4. Conclusion

The experimental results demonstrated a simple and effective method for improving the mechanical performance of adhesively bonded joints between carbon fibre composites and aluminium alloys. Through alkaline etching treatments for aluminium substrates, the weak passive oxide layers were removed. This allowed the formation of nanoscale thin hydroxide layers on the substrates, which helped achieve higher SFEs compared to those of untreated samples. The surface topography and roughness parameters were strongly dependant on the concentration of NaOH. The single lap shear tests performed on the etched samples showed maximum increases of 91% in bond strength. These failed surfaces also presented partial adhesive and substrate failures on composite sides, which indicated improvements in the interfacial bonding strength between adhesive and aluminium. Before applying high-viscosity adhesives to the micro-rough NaOH-treated aluminium surfaces, the RPC technique could ensure intimate contact and further increase the interfacial bonding strength. The combination of NaOH-treatment and RPC appears to be effective and is simple enough to be adopted in industrial applications.

Conflicts of interest

The authors declared that they have no conflicts of interest to this work.

Acknowledgement

This work was supported by the Australian Government Research Training Program. The authors acknowledge the facilities, and the scientific and technical assistance of the Australian Microscopy & Microanalysis Research Facility at the Centre for Microscopy, Characterisation & Analysis, The University of Western Australia, a facility funded by the University, State and Commonwealth Governments.

Appendix A. Supplementary data

Supplementary data to this article can be found online at https://doi.org/10.1016/j.compositesb.2019.107478.

References

[1] Banea MD, Rosioara M, Carbas RJC, da Silva LFM. Multi-material adhesive joints for automotive industry. Compos B Eng 2018;151:71–7.
[2] Qin G, Na J, Mu W, Tan W, Yang J, Ren J. Effect of continuous high temperature exposure on the adhesive strength of epoxy adhesive, CFRP and adhesively bonded CFRP-aluminum alloy joints. Compos B Eng 2018;154:43–55.
[3] Hamill L, Nutt S. Adhesion of metallic glass and epoxy in composite-metal bonding. Compos B Eng 2018;134:186–92.
[4] Liu X, Shao X, Li Q, Sun G. Failure mechanisms in carbon fiber reinforced plastics (CFRP)/aluminum (Al) adhesive bonds subjected to low-velocity transverse pre-impact following by axial post-tension. Compos B Eng 2019;172:339–51.
[5] Sun G, Li S, Li G, Li Q. On crashing behaviors of aluminium/CFRP tubes subjected to axial and oblique loading: an experimental study. Compos B Eng 2018;145:47–56.
[6] Li N, Li Y, Zhou J, He Y, Hao X. Drilling delamination and thermal damage of carbon nanotube/carbon fiber reinforced epoxy composites processed by microwave curing. Int J Mach Tool Manuf 2015;97:11–7.
[7] Isbilir O, Ghassemieh E. Numerical investigation of the effects of drill geometry on drilling induced delamination of carbon fiber reinforced composites. Compos Struct 2013;105:126–33.
[8] Ismail SO, Ojo SO, Dhakal HN. Thermo-mechanical modelling of FRP cross-ply composite laminates drilling: delamination damage analysis. Compos B Eng 2017;108:45–52.
[9] Mandel M, Krüger L. Determination of pitting sensitivity of the aluminium alloy EN AW-6060-T6 in a carbon-fibre reinforced plastic/aluminium rivet joint by finite element simulation of the galvanic corrosion process. Corros Sci 2013;73:172–80.
[10] Håkansson E, Hoffman J, Predecki P, Kumosa M. The role of corrosion product deposition in galvanic corrosion of aluminum/carbon systems. Corros Sci 2017;114:10–6.
[11] Fiore V, Calabrese L, Proverbio E, Passari R, Valenza A. Salt spray fog ageing of hybrid composite/metal rivet joints for automotive applications. Compos B Eng 2017;108:65–74.
[12] Wu C, Chen C, He L, Yan W. Comparison on damage tolerance of scarf and stepped-lap bonded composite joints under quasi-static loading. Compos B Eng 2018;155:19–30.
[13] Sun Z, Shi S, Hu X, Guo X, Chen J, Chen H. Short-aramid-fiber toughening of epoxy adhesive joint between carbon fiber composites and metal substrates with different surface morphology. Compos B Eng 2015;77:38–45.
[14] Sun Z, Jeyaraman J, Shi S, Sun S, Hu X, Chen H. Processing and property of carbon-fiber aluminum-foam sandwich with aramid-fiber composite adhesive joints. J Adhes Sci Technol 2014;28:1835–45.
[15] Salgin B, Özkanat Ö, Mol JMC, Terryn H, Rohwerder M. Role of surface oxide properties on the aluminum/epoxy interfacial bonding. J Phys Chem C 2013;117:4480–7.
[16] Kwon D-J, Kim J-H, Kim Y-J, Kim J-J, Park S-M, Kwon I-J, et al. Comparison of interfacial adhesion of hybrid materials of aluminum/carbon fiber reinforced epoxy composites with different surface roughness. Compos B Eng 2019;170:11–8.
[17] Arenas JM, Alía C, Narbón JJ, Ocaña R, González C. Considerations for the industrial application of structural adhesive joints in the aluminium–composite material bonding. Compos B Eng 2013;44:417–23.
[18] Wang B, Hu X, Lu P. Improvement of adhesive bonding of grit-blasted steel substrates by using diluted resin as a primer. Int J Adhesion Adhes 2017;73:92–9.
[19] Jang S, Chung J, Seo S, Lee S, Lee Y, Lee S, et al. Enhancement of interfacial adhesion based on nanostructured alumina/aluminum laminates. Compos B Eng 2017;129:204–9.
[20] Wang B, Hu X, Hui J, Lu P, Jiang B. CNT-reinforced adhesive joint between grit-blasted steel substrates fabricated by simple resin pre-coating method. J Adhes 2018;94:529–40.
[21] Abouarkoub A, Thompson G, Zhou X, Scamans G. The influence of heat treatment on the caustic etching behaviour of the automotive AA6111 alloy. J Miner Mater Charact Eng 2016;04:364.
[22] Saleema N, Sarkar DK, Paynter RW, Gallant D, Eskandarian M. A simple surface treatment and characterization of AA 6061 aluminum alloy surface for adhesive bonding applications. Appl Surf Sci 2012;261:742–8.
[23] Zain NM, Ahmad SH, Ali ES. Effect of surface treatments on the durability of green polyurethane adhesive bonded aluminium alloy. Int J Adhesion Adhes 2014;55:43–55.
[24] Ebnesajjad S, Landrock AH. Adhesives Technology handbook. William Andrew; 2014.
[25] Paz E, Narbón JJ, Abenojar J, Cledera M, Real JC del. Influence of acrylic adhesive viscosity and surface roughness on the properties of adhesive joint. J Adhes 2016;92:877–91.
[26] Liu W, Zheng Y, Hu X, Han X, Chen Y. Interfacial bonding enhancement on the epoxy adhesive joint between engineered bamboo and steel substrates with resin pre-coating surface treatment. Wood Sci Technol 2019;53:785–99.
[27] Han X, Yuan B, Tan B, Hu X, Chen S. Repair of subsurface micro-cracks in rock using resin pre-coating technique. Constr Build Mater 2019;196:485–91.
[28] Liu DZ, Jindal S, Amamcharla J, Anand S, Metzger L. Short communication: evaluation of a sol-gel–based stainless steel surface modification to reduce fouling and biofilm formation during pasteurization of milk. J Dairy Sci 2017;100:2577–81.
[29] Doru MO, Özel A, Akpinar S, Aydin MD. Effect of the spew fillet on adhesively bonded single-lap joint subjected to tensile loading: experimental and 3-D non-linear stress analysis. J Adhes 2014;90:195–209.

[30] Akpinar S, Doru MO, Özel A, Aydin MD, Jahanpasand HG. The effect of the spew fillet on an adhesively bonded single-lap joint subjected to bending moment. Compos B Eng 2013;55:55–64.
[31] Ahmad H, Crocombe AD, Smith PA. Strength prediction in CFRP woven laminate bolted single-lap joints under quasi-static loading using XFEM. Compos Appl Sci Manuf 2014;66:82–93.
[32] Garcia-Garcia FJ, Skeldon P, Thompson GE, Smith GC. The effect of nickel on alloy microstructure and electrochemical behaviour of AA1050 aluminium alloy in acid and alkaline solutions. Electrochim Acta 2012;75:229–38.
[33] Çapraz ÖÖ, Ide S, Shrotriya P, Hebert KR. Tensile stress and plastic deformation in aluminum induced by aqueous corrosion. Acta Mater 2016;115:434–41.
[34] Goushegir SM, Scharnagl N, J F, Santos dos, Amancio-Filho ST. XPS analysis of the interface between AA2024-T3/CF-PPS friction spot joints. Surf Interface Anal 2016;48:706–11.
[35] Uhart A, Ledeuil J-B, Gonbeau D, Dupin J-C, Bonino J-P, Ansart F, et al. An Auger and XPS survey of cerium active corrosion protection for AA2024-T3 aluminum alloy. Appl Surf Sci 2016;390:751–9.
[36] Li X, Hufnagel S, Xu H, Valdes SA, Thakkar SG, Cui Z, et al. Aluminum (oxy) hydroxide nanosticks synthesized in bicontinuous reverse microemulsion have potent vaccine adjuvant activity. ACS Appl Mater Interfaces 2017;9:22893–901.
[37] Din RU, Gudla VC, Jellesen MS, Ambat R. Accelerated growth of oxide film on aluminium alloys under steam: Part I: effects of alloy chemistry and steam vapour pressure on microstructure. Surf Coat Technol 2015;276:77–88.
[38] Seo YI, Lee YJ, Kim D-G, Lee KH, Kim YD. Mechanism of aluminum hydroxide layer formation by surface modification of aluminum. Appl Surf Sci 2010;256:4434–7.
[39] Kubiak KJ, Wilson MCT, Mathia TG, Carval Ph. Wettability versus roughness of engineering surfaces. Wear 2011;271:523–8.
[40] Kosior D, Kowalczuk PB, Zawala J. Surface roughness in bubble attachment and flotation of highly hydrophobic solids in presence of frother – experiment and simulations. Physicochem Probl Miner Process 2017;54:63–72.
[41] Yang G, Yang T, Yuan W, Du Y. The influence of surface treatment on the tensile properties of carbon fiber-reinforced epoxy composites-bonded joints. Compos B Eng 2019;160:446–56.
[42] Budhe S, Ghumatkar A, Birajdar N, Banea MD. Effect of surface roughness using different adherend materials on the adhesive bond strength. Appl Adhes Sci 2015;3:20.
[43] Ghumatkar A, Budhe S, Sekhar R, Banea MD, Barros S de, Ghumatkar A, et al. Influence of adherend surface roughness on the adhesive bond strength. Lat Am J Solid Struct 2016;13:2356–70.
[44] Boutar Y, Naïmi S, Mezlini S, L FM, Silva da, Hamdaoui M, Ali MBS. Effect of adhesive thickness and surface roughness on the shear strength of aluminium one-component polyurethane adhesive single-lap joints for automotive applications. J Adhes Sci Technol 2016;30:1913–29.
[45] Liu Q, Xu X, Ma J, Wang J, Shi Y, Hui D. Lateral crushing and bending responses of CFRP square tube filled with aluminum honeycomb. Compos B Eng 2017;118:104–15.
[46] Wu Y, Liu Q, Fu J, Li Q, Hui D. Dynamic crash responses of bio-inspired aluminum honeycomb sandwich structures with CFRP panels. Compos B Eng 2017;121:122–33.
[47] Sun Z, Shi S, Guo X, Hu X, Chen H. On compressive properties of composite sandwich structures with grid reinforced honeycomb core. Compos B Eng 2016;94:245–52.
[48] Banea MD, da Silva LFM. The effect of temperature on the mechanical properties of adhesives for the automotive industry. Proc IMechE 2010;224:51–62.
[49] Hua Y, Gu L, Trogdon M. Three-dimensional modeling of carbon/epoxy to titanium single-lap joints with variable adhesive recess length. Int J Adhesion Adhes 2012;38:25–30.